

# Matching Contactless and Contact-based Conventional Fingerprint Images for Biometrics Identification

Chenhao Lin, Ajay Kumar

**Abstract**—Vast databases of billions of contact-based fingerprints have been developed to protect national borders and support e-governance programs. Emerging contactless fingerprint sensors offer better hygiene, security and accuracy. However the adoption/success of such contactless fingerprint technologies largely depends on advanced capability to match contactless 2D fingerprints with legacy contact-based fingerprint databases. This paper investigates such problem and develops a new approach to accurately match such fingerprint images. Robust thin-plate spline (RTPS) is developed to more accurately model elastic fingerprint deformations using splines. In order to correct such deformations on the contact-based fingerprints, RTPS based generalized fingerprint deformation correction model (DCM) is proposed. The usage of DCM results in accurate alignment of key minutiae features observed on the contactless and contact-based fingerprints. Further improvement in such cross-matching performance is investigated by incorporating minutiae related ridges. We also develop a new database of 1800 contactless 2D fingerprints and the *corresponding* contact-based fingerprints acquired from 300 clients which is made publicly accessible for further research. The experimental results presented in this paper, using two publicly available databases, validate our approach and achieve outperforming results for matching contactless 2D and contact-based fingerprint images.

**Index Terms**—Contactless fingerprint sensor interoperability, Biometrics, Deformation correction model (DCM).

## I. INTRODUCTION

FINGERPRINTS is the most popular biometrics modality widely used by the law-enforcement departments and national ID programs around the world [1]. It offers high level of uniqueness, accuracy and permanence which has attracted wide range of applications in e-governance, law-enforcement and e-business [2]. Since more and more centralized identification systems are increasingly deployed for fingerprint identification which can receive fingerprint images acquired from different kinds of fingerprint sensors, the fingerprint sensor interoperability problem has attracted growing attention [3]. For example, large scale fingerprint systems Aadhaar system [4] matches fingerprints from over a billion of different subjects that are acquired using wide variety of sensors [5].

In recent years, contactless fingerprint identification systems have been introduced for better hygiene, security and to overcome the limitations from traditional contact-based fingerprint identification systems. Contact-based fingerprint sensors have to cope up with hygienic concerns, sensor surface noise, latents from previous impression, and fingerprint deformation due to improper placement or uneven distribution of pressure [6]. As a result full potential from the fingerprint modality is not yet to be realized. On the other hand, contactless fingerprint imaging can preserve and recover the ground truth information without the deformation. Therefore much higher matching accuracy can be expected from the contactless fingerprints

than those from the contact-based fingerprint identification. Although more and more contactless fingerprint identification systems have been developed [7]–[10], [40], there has been almost no or nil attention for the development of algorithms to enhance interoperability between contact-based and contactless fingerprint sensors. Instead of investigating on the development of algorithms for more accurate contactless fingerprint identification, our focuses on improving accuracy for matching contactless to contact-based fingerprint to advance interoperability of emerging contactless fingerprint technologies. The success of emerging contactless fingerprint sensors largely depends on their capability to match with legacy fingerprint database images. Therefore it is important to develop specialized algorithms to improve fingerprint sensor interoperability between the contact-based and the contactless fingerprint sensors.

It is well-known that the elastic deformations are inherent on images acquired from the contact-based fingerprint sensors and this is the key source of degradation in accuracy of matching fingerprints. Several methods have been detailed in the literature [12]–[17] to address the fingerprint deformation problems. Among these, the approaches in [15], [16] and [17] estimate the deformations using thin-plate spline (TPS) model [18] and have illustrated outperforming results for the fingerprint deformation correction. However these methods cannot be considered as reliable because they use thin-plate spline model to estimate and correct fingerprint deformations from the template and query fingerprint images, while both of these have been acquired from contact-based sensors, which themselves suffer from the elastic deformations. Several promising methods to achieve fingerprint sensor interoperability and estimate/correct fingerprint deformations have been proposed in the literature. However this area requires further attention as the review of earlier works underline following limitations:

- There has been almost nil attention to develop effective algorithms to accurately match fingerprint images acquired from the contactless and contact-based fingerprint sensors, i.e., ensure interoperability between contact-based and contactless fingerprints. The fingerprint matching algorithms introduced in the literature to match fingerprint images from different fingerprint sensors or with rolled fingerprint images deliver very limited performance when employed for matching contact-based fingerprints with contactless 2D fingerprint images.
- The methods that use TPS model to correct the fingerprint deformations on the contact-based fingerprints [14], [15], [17] are computationally complex and fail to correct the fingerprint deformations *relativeto* the ground truth. As a result, the fingerprint matching techniques introduced in

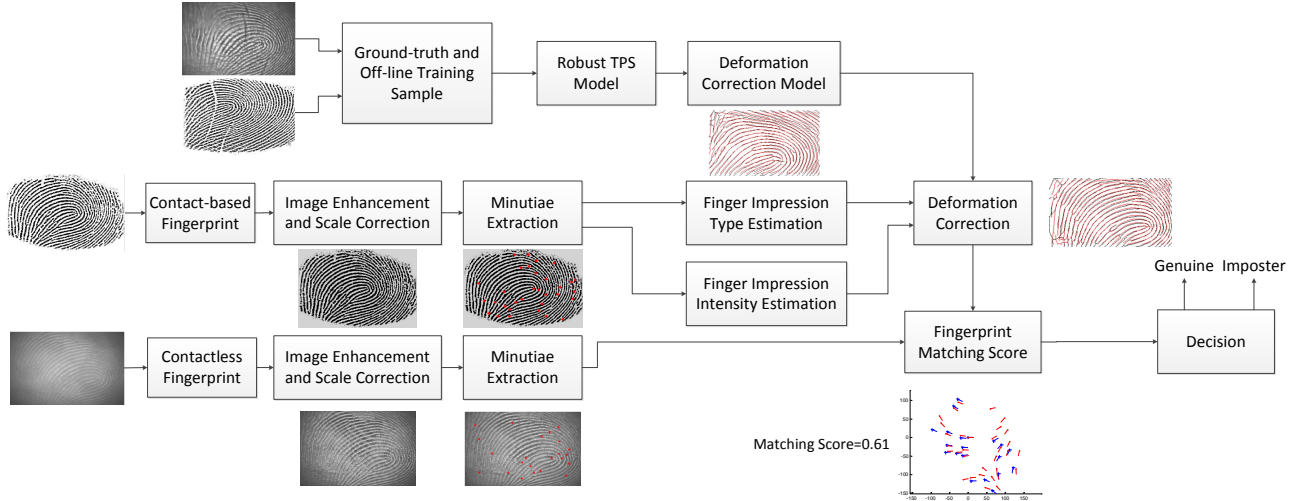


Fig. 1: Block diagram for the contactless to contact-based fingerprint matching approach using deformation correction model.

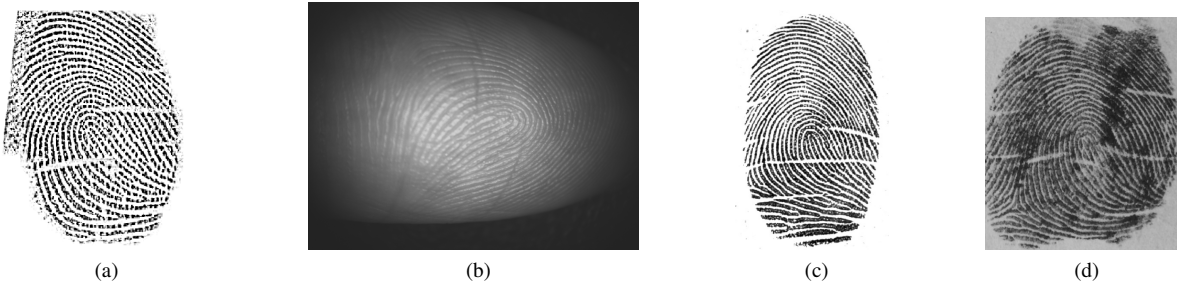


Fig. 2: Same fingerprint acquired from different sensors. (a) Contact-based fingerprint from Digital Persona (b) Contactless fingerprint from contactless camera (c) Contact-based fingerprint from Futronic (d) Rolled fingerprint.

the literature, for cross-sensor fingerprint matching, only can deliver limited improvement in performance while matching fingerprint images acquired from contact-based and contactless fingerprints sensors.

#### A. Our Work and Contributions

This paper investigates the problem of fingerprint sensor interoperability when the images from the same fingers are acquired using the contact-based and contactless fingerprint sensors [40]. Contactless imaging inherently introduces scale, rotational and spatial variations in three dimensional spaces and therefore this problem is more challenging *than* fingerprint sensor interoperability for two contact-based sensors which has received more attention in the literature. The key contributions of this paper are summarized in the following:

- A *robust thin-plate spline (RTPS)* model for accurate localization of key points to accurately match for contactless to contact-based fingerprints is proposed. Unlike traditional TPS interpolation approach, our model attempts to minimize the localization errors for all the key points many of which can appear in the unregistered test images (more details in section III-A). Our experimental results (Fig 5, 11) suggest more accurate data interpolation by using proposed *RTPS* model than using traditional TPS model [18] or approximating TPS model [19].
- A generalized fingerprint impression *deformation correction model (DCM)* is developed using robust thin-plate spline by comparing contact-based fingerprint impressions

with several contactless fingerprint (ground truth) impressions from the same finger. We used this model on each of the unknown contact-based fingerprints to achieve better alignment with the corresponding contactless fingerprint. This method is significantly different from the methods in [15] and [16] which highly rely on accurate extraction of minutiae. Our method is more robust and offers faster and more accurate fingerprint deformation correction (more details are in section III-D).

- This paper has also developed a database of 2D contactless fingerprint images and their corresponding contact-based fingerprint images [20]. This database consists of 1800 fingerprint images acquired from 300 clients and is made available in the public domain to advance much needed research in this area.

The block diagram of the proposed contactless to contact-based (cross) fingerprint matching approach is illustrated in Fig 1. A triangulation based fingerprint method is developed for contact-based and contactless fingerprints scale correction. The *RTPS* model developed in this paper is used to offline train a generalized contact-based fingerprint impression deformation correction model. Contact-based fingerprint impression types and intensity are automatically estimated. Based on these estimations, appropriate pre-trained deformation correction model is used to correct the deformations in the contact-based fingerprints. The minutiae features are employed for the global fingerprint alignment and matching.

## B. Related Work

Research on fingerprint sensor interoperability has attracted considerable attention in the literature as a wide variety of contact-based fingerprint sensors are deployed worldwide. Reference [3] investigated fingerprint sensor interoperability problem for two different flat (plain) fingerprint sensors and examined the extent of degradation in the matching accuracy when images from two such different sensors are matched. Reference [21] details a series experiments on plain-to-rolled fingerprint identification and demonstrated that it can be more difficult than matching plain-to-plain fingerprints. Alonso et al. [22] investigated fingerprint sensor interoperability and sensor fusion using a multi-sensor fingerprint database acquired from three different fingerprint sensors including thermal and optical sensors. The experimental results in this reference also illustrate that the matching performance drops dramatically when fingerprints acquired from different sensors are matched. The technical report in [23] also investigates fingerprint sensor interoperability problem using the fingerprints acquired from nine different sensors including one thermal sensor, four capacitive sensors and four optical sensors. The work detailed in above references is quite promising but limited to addressing the fingerprint sensor interoperability problem only for the contact-based fingerprints acquired from different sensors. It is more challenging, meaningful and relevant, in view of recent technological advances, to match contact-based fingerprint images in legacy fingerprint databases with the contactless fingerprints sensors.

References [24], [25] described the unwrapping of 3D touchless fingerprints to achieve compatibility for unwrapped touchless fingerprints with the legacy rolled fingerprint images. Authors have used a commercial *matcher* to evaluate the matching performance for touchless rolled impressions and contact-based rolled fingerprints. Although these promising but preliminary studies have investigated the interoperability problem between *unwrapped* touchless fingerprints and contact-based *rolled* fingerprints, the focus of problem investigated is different. Contactless rolled fingerprint acquisitions have higher bulk and cost as it requires multiple cameras to recover contactless rolled fingerprints. Therefore contactless fingerprints that are generate 2D images equivalent to those from popular flat fingerprint sensors is considered in this work as they provide low-cost and flexible alternative to contact-based fingerprint sensors. Also the work in [24], [25] should be considered preliminary on a limited size proprietary database, i.e. reference [24] uses images from 38 fingers with two samples while reference [25] uses images from 102 fingers with two samples, and there has been no attempt to correct the deformations in the rolled fingerprints. The technical reports in [26], [27] and the references [37], [41] describe outcome from a range of experiments that were designed to investigate the matching performance and interoperability of contact-based and contactless fingerprints (rolled and unwrapped fingerprints) acquired from a variety of commercial fingerprint sensors. These experimental results also indicate significant degradation in the matching performance when the fingerprint images acquired from a contactless fingerprint sensor were

matched with the respective fingerprint images acquired using contact-based commercial fingerprint sensor. These references provide very interesting insights on the interoperability among the contact-based and contactless fingerprint devices; however, these are only evaluation reports and do not make any attempt/research to further improve interoperability or correct the deformations in contact-based fingerprint images that could help to improve such cross matching accuracy.

In order to address inherent deformations in the contact-based fingerprints, several approaches have been proposed in the literature. In [13] a plastic distortion model is proposed to address the non-linear deformations in contact-based fingerprints. Although the results demonstrated its efficiency in minutiae extraction from fingerprints with higher deformations, authors did not perform any experiments for the fingerprints matching using the proposed model. The conference version of this paper [40] has also evaluated performance degraded resulted from contact-based fingerprint deformation and provided preliminary results for improving contact-based to contactless fingerprint interoperability. Reference [28] presents an automated approach to remove fingerprint deformations by using an *inverse distortion transform* model. This work has some promises but it fails to model the fingerprint deformation by comparing it with the ground truth. Some publications have also discussed the distortion on contactless fingerprint images. Reference [42] proposed an approach to address perspective distortion and rotation effect on contactless fingerprint in less controlled applications, like mobile devices. The experimental results on the contactless fingerprints database with intentional rotation indicate that such proposed approach can improve recognition performance by directly using minutiae-based matching. However, this paper incorporates neural network which generally require large training samples which is the key limitation for the application of this method.

The thin-plate splines (TPS) model has demonstrated its effectiveness for the deformation correction in contact-based fingerprints. There are few publications that have investigated this model to correct fingerprint deformation and illustrated promising results. In [15], thin-plate spline model was introduced to describe the deformation in fingerprints. For each of the two fingerprints, local minutiae are extracted for the deformation correction and global minutiae are used for further refining the correction. Then fingerprints are matched using the corrected global minutiae features. This method was introduced for the first time to correct minutiae deformations by using approximating TPS model [19] and achieved promising matching performance. However this method is highly relies on the accurate extraction of minutiae and due to the iterative selection of the matching thresholds the computational complexity of this method is also high. Reference [16] proposed an average deformation model to correct fingerprint impressions deformation. Authors applied thin-plate spline model on multiple fingerprint impressions from the same fingers and estimated average deformation of the fingerprints. Similar to [16], authors in [14] proposed a thin-plate spline calibration model to address fingerprint sensor interoperability. The average deformation model was trained

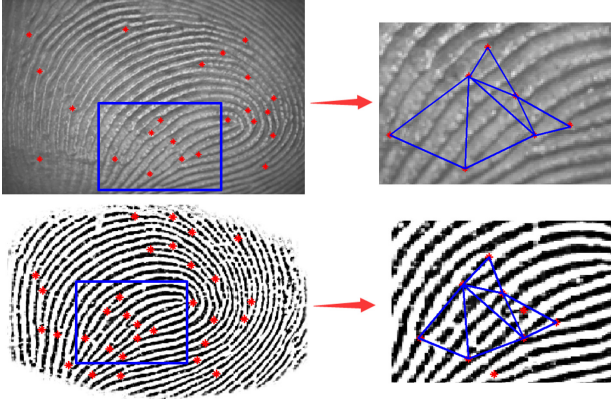


Fig. 3: Similar triangle samples from contactless and contact-based fingerprint. Red point represents the minutiae.

to correct the deformations of fingerprints from the different sensors. However this method is highly computationally complex as it requires computations for different parameters of the average deformation model. Their template fingerprint and query fingerprint are both 2D contact-based fingerprints and therefore have distortions. Therefore the model trained from the fingerprint images, which themselves have deformations, cannot be expected to be reliable. In addition, the TPS model [18] employed in most references lacks robustness since the localization errors for the transformed points are not estimated.

## II. SENSOR INTEROPERABILITY AND DATA PROCESSING

Fingerprint sensor interoperability refers to the capability for accurately matching the fingerprint images that are acquired using different fingerprint sensors. As discussed in several publications, the matching accuracy from fingerprint identification systems dramatically degrades when the fingerprint images acquired from the different contact-based/contactless sensors are matched. Sensor interoperability between the contact-based and contactless fingerprint sensors is among the most challenging problems but has attracted very little attention from the researchers. With the increasing development and deployment of contactless fingerprint identification systems, in depth study on contact-based and contactless fingerprint sensor interoperability becomes important and meaningful. As illustrated in Fig 2 (a)-(b), our study uses the fingerprint images acquired from same subject/finger using different contact-based and contactless sensors.

As a first step for contact-based and contactless fingerprint cross-matching, fingerprint image enhancement and fingerprint scale normalization is performed on each of the acquired images. The original resolution of contactless fingerprint image and the corresponding contact-based fingerprint image is  $1400 \times 900$  and  $356 \times 328$  pixels. In order to enhance the contrast of contactless fingerprint ridge and valley, adaptive histogram equalization [29] is performed. The contact-based fingerprints are then rotated 90 degrees counter clockwise followed by a horizontal flip (Fig 2). Fingerprint scaling is essential to address sensor interoperability problem. Several methods [30], [31] for fingerprint scale normalization have been developed to improve the performance from fingerprints cross-matching. In this paper, we propose a simple but efficient

method that uses fingerprint minutiae triangulations to align contactless and contact-based fingerprints into same scaling ratio. In [31], Delaunay triangulation based fingerprint scaling is proposed. This method fails to recover or match Delaunay triangles when false or missing minutiae are extracted as the features. This has motivated us to develop a more robust and automated approach for the fingerprint scale normalization by using minutiae triangulations. Firstly the contactless fingerprint is resized to  $350 \times 225$  using bilinear interpolation. Then minutiae are extracted from each contact-based fingerprint and contactless fingerprint using [32] and minutiae triangles are extracted based on each three minutiae ( $m_1, m_2, m_3$ ). Similar to ISO/IEC minutiae template [33], fingerprint minutia template can be represented as  $m = [x, y, \theta, q, t]$ , where  $x, y$  specifies the minutiae location,  $\theta$  is the minutia direction,  $q$  is the minutia quality and  $t$  is the type of minutia (ridge ending or ridge bifurcation). Triangle features can be represented as:

$$\left[ \varphi, \frac{l_{max}}{l_{s\_max}}, \frac{l_{max}}{l_{min}}, \tilde{\theta}_{max}, \tilde{\theta}_{min} \right] \quad (1)$$

where  $\varphi$  is the largest angle in the triangulation,  $l_{max}$  and  $l_{min}$  represent the largest side and smallest side respectively.  $l_{s\_max}$  is the second largest side.  $\tilde{\theta} = \theta_1 - \theta_2$  is differences of minutiae direction while  $\tilde{\theta}_{max}$  represents the orientation difference between two minutiae of the largest side  $l_{max}$ . Based on the invariant features representation in (1), similar triangles can be computed as in the following.

$$\Delta\varphi = \left| \varphi_{Pi} - \varphi_{Qj} \right| \quad (2)$$

$$\Delta l_1 = \left| \frac{l_{Pimax}}{l_{Pis\_max}} - \frac{l_{Qjmax}}{l_{Qjs\_max}} \right|, \Delta l_2 = \left| \frac{l_{Pimin}}{l_{Pimin}} - \frac{l_{Qjmin}}{l_{Qjmin}} \right| \quad (3)$$

$$\Delta\tilde{\theta}_{max} = \left| \tilde{\theta}_{Pimax} - \tilde{\theta}_{Qjmax} \right|, \Delta\tilde{\theta}_{min} = \left| \tilde{\theta}_{Pimin} - \tilde{\theta}_{Qjmin} \right| \quad (4)$$

where  $P$  and  $Q$  represent the triangulations of contactless fingerprint and contact-based fingerprint respectively. If  $\Delta\varphi$ ,  $\Delta l_1$ ,  $\Delta l_2$ ,  $\Delta\tilde{\theta}_{max}$ , and  $\Delta\tilde{\theta}_{min}$  are smaller than pre-determined threshold, two triangulations can be considered as similar triangulations. The scale value  $sl$  can be estimated by computing the average scale of the corresponding sides of two similar triangulations.

$$sl = \frac{1}{3} \left( \frac{l_{Pimax}}{l_{Qjmax}} + \frac{l_{Pis\_max}}{l_{Qjs\_max}} + \frac{l_{Pimin}}{l_{Qjmin}} \right) \quad (5)$$

In order to exclude the outliers or the influence from spurious minutiae, we automatically exclude scale values if they are smaller or larger than predetermined threshold. We then use the mean scale value  $sl_{mean}$  computed from all possible similar triangles, excluding the outliers, as the scale factor between contactless and contact-based fingerprint images. The algorithm for cross fingerprints scale normalization can be summarized as shown in algorithm 1. Fig 3 illustrates image samples from the same subject/finger, with their automatically extracted triangulation samples, that are used to compute scale factor for the image normalization.

---

**Algorithm 1** Computing Scale Factor for Normalization
 

---

**Input:** Contactless and contact-based fingerprints  $CL$ ,  $CB$  and corresponding triangulations  $P$  and  $Q$ .

**Output:** Mean scale values  $sl_{max}$  for cross fingerprints

```

1: for each triangulation  $P_i$  in  $P$  do
2:   extract minutiae triangulation features (1);
3:   for each triangulation  $Q_j$  in  $Q$  do
4:     extract minutiae triangulation features (1);
5:     if equation (2), (3), (4) < Threshold then
6:       compute scale value  $sl_n$  using (5)
7:     end if
8:   end for
9: end for
10: for  $n$  similar triangulations in  $P$  and  $Q$  do
11:    $sl_{mean} = \text{sum}(sl_n)/n$ 
12: end for

```

---

### III. FINGERPRINT DEFORMATION CORRECTION

The fingerprint scale correction algorithm described in previous section results in better alignment between the contactless and contact-based fingerprint images. However this is not adequate to correct the nonlinear deformations in the contact-based fingerprint images. Such deformations can seriously degrade the matching performance, especially for the cross-matching between contactless and contact-based fingerprints. Thin-plate spline (TPS) model [18] and approximating TPS [19] are widely used to correct elastic deformation. In this paper, we presented a more robust thin-plate spline (RTPS) model by minimizing transformed points localization errors. Based on RTPS, a generalized fingerprint deformation correction model (DCM) is proposed. It may be noted that the influence of perspective distortion is more pronounced at a distance away from image center. As also presented in many references (e.g. [10]) the useful region of interest (ROI) in contactless fingerprint reduces and it is reasonable to ignore the perspective distortion in such region of interest near image center. Therefore, in this work, ROI of contactless fingerprint image was used for training and testing the deformation correction model as the perspective distortion in the contactless fingerprint images is assumed to be significantly small. It is judicious to consider the contactless fingerprint as the ground truth since such images are not expected to have any deformations, particular near the image center or region of interest used in our work. Each of the contact-based fingerprint images are corrected for the deformations using the transformation correction model detailed in following sub sections.

#### A. Robust Thin-plate Spline Model

Thin plate splines (TPS) represent a spline-based technique for the data interpolation and smoothing. Let  $(x_i, y_i)$  denote the original minutiae location of contact-based fingerprint and  $(x'_i, y'_i)$  be the transformed locations of contactless fingerprint. This relationship can be described by TPS interpolation function:

$$(x', y') = f(x, y) \quad (6)$$

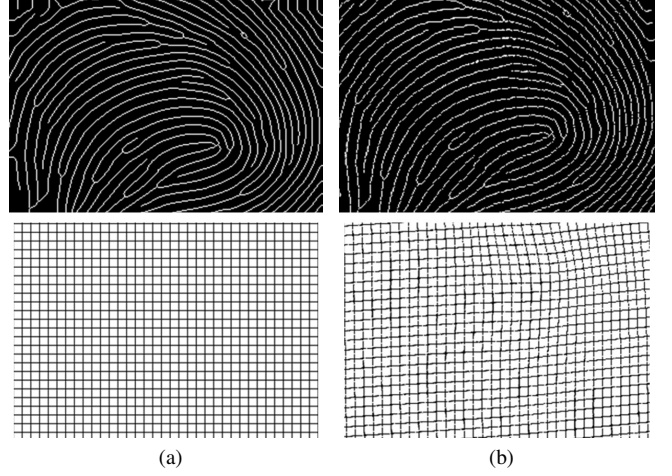


Fig. 4: (a) Original contact-based fingerprint skeleton and its reference grid. (b) Contact-based fingerprint skeleton with deformation correction and its reference grid.

$$f(x, y) = a_1 + a_2x + a_3y + \sum_{i=1}^n w_i U(\|(x_i, y_i) - (x, y)\|) \quad (7)$$

where  $\mathbf{a} = (a_1, a_2, a_3)$  defines affine transformation and  $\mathbf{w}$  represents additional deformation.  $U(\|(x_i, y_i) - (x, y)\|)$  is the basis function. The function  $f$  minimizes the bending energy,

$$J_f = \iint_{R^2} (f_{xx}^2 + f_{xy}^2 + f_{yy}^2) dx dy \quad (8)$$

The parameters of  $f$  can be recovered from the solution of the following equation,

$$\mathbf{K}\mathbf{w} + \mathbf{P}\mathbf{a} = \mathbf{v}, \mathbf{P}^T \mathbf{w} = 0 \quad (9)$$

where the  $i^{th}$  element of  $\mathbf{K}$  is  $U(\|(x_i, y_i) - (x, y)\|)$ , the  $i^{th}$  row of  $\mathbf{P}$  is  $(1, x_i, y_i)$ , the  $i^{th}$  element of  $\mathbf{v}$  is  $(x'_i, y'_i)$ ,  $\mathbf{w} = [w_1, \dots, w_n]^T$  and  $\mathbf{a} = [a_1, a_2, a_3]^T$ .

The use of conventional thin-plate spline interpolation approach [18] on contact-based fingerprint images can help to accurately transform the landmark (manually marked minutiae location) points. However in addition to these landmarks, the other possible points, that can be key points or ridges on other unregistered test images, that cannot be accurately aligned with ground truth. In order to achieve more accurate transformation, it is therefore necessary to incorporate a model that can minimize the transformed points localization errors. Such model is referred here as RTPS and the localization error can be modeled using the following equation,

$$E_{error} = \sum_{j=1}^m \|(x'_j, y'_j) - f(x_j, y_j)\| \quad (10)$$

where  $(x_j, y_j)$  is marked minutiae location in contact-based fingerprint.  $(x'_j, y'_j)$  is marked transformed minutiae locations for contactless fingerprint.  $m$  is the number of marked points that used for evaluating TPS accuracy. The bending energy function for the proposed RTPS can be represented as,

$$J_{Rf} = \iint_{R^2} (f_{xx}^2 + f_{xy}^2 + f_{yy}^2) dx dy + E_{error} \quad (11)$$

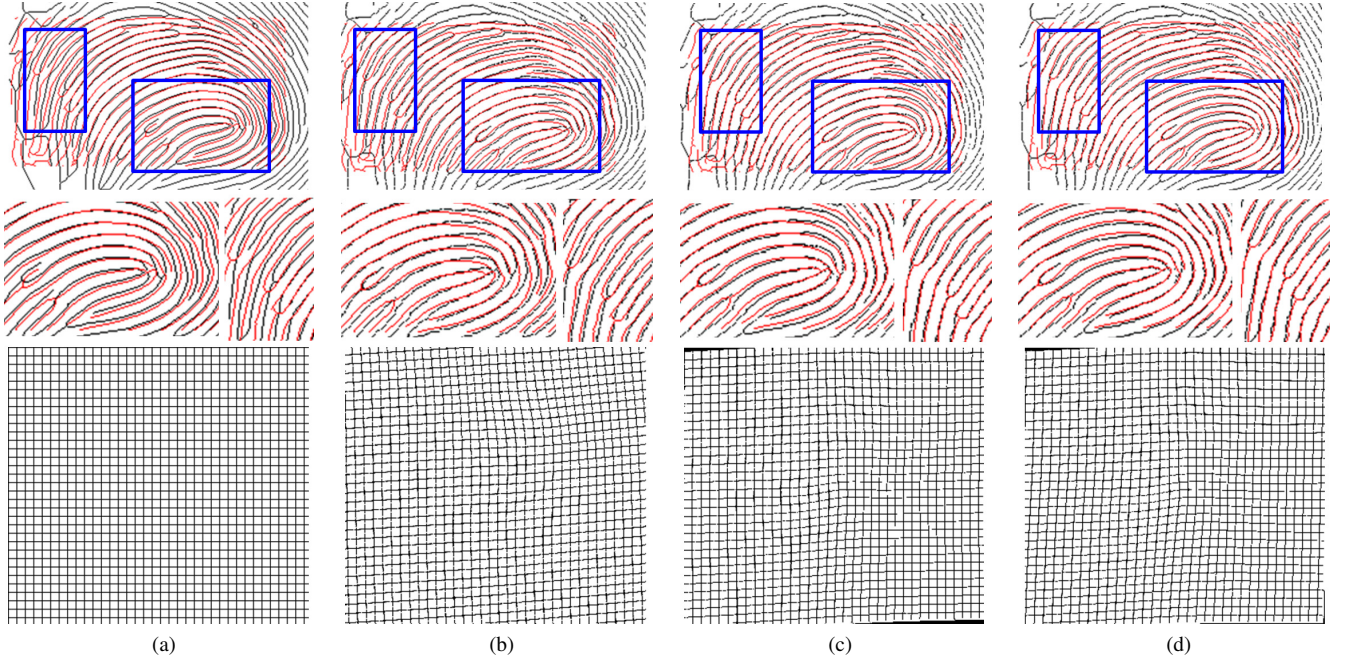


Fig. 5: Red skeleton represents contactless fingerprint, black skeleton represents contact-based fingerprint and corresponding reference grid (a) Fingerprint alignment without correction (b) Fingerprint alignment using TPS (c) Fingerprint alignment using proposed model and iteration number is 5 (d) Fingerprint alignment using proposed model and iteration number is 8.

The parameters of  $f$  can be recovered from the solution of the following equation,

$$(\mathbf{K} + \mathbf{E})\mathbf{w} + \mathbf{P}\mathbf{a} = \mathbf{v}, \mathbf{P}^T \mathbf{w} = 0 \quad (12)$$

where  $\mathbf{K}$ ,  $\mathbf{P}$  and  $\mathbf{v}$  are same as (9).  $\mathbf{E}$  is a matrix with some initial parameter ( $\omega$ ) to minimize  $E_{error}$ . The  $j^{th}$   $\mathbf{E}$  is:

$$\mathbf{E}_j = U(\| (x_j, y_j) - (x, y) \| + \omega_j \| (x_j, y_j) - (x, y) \|) \quad (13)$$

$\omega_j$  is initial parameter which is empirically selected in the range of 0 to 0.3. A close fit between this model or  $\omega_j$  to minimize the error  $E_j$  is achieved in a number of iterations. The value of  $E_{error}$  and  $\omega$  are initialized to zero for computing original TPS function. Then marked location  $(x_j, y_j)$  is transformed using original TPS function and  $E_{error}$  is calculated. Next, the original landmarks with the corresponding  $\omega_j$  are also transformed to generate new transformation matrix and marked location  $(x_j, y_j)$  is transformed to compute new  $E_{error}$ . The process is repeated until  $E_{error}$  is stabilized or doesn't decrease in the next three iterations.

### B. Deformation Correction Model

Based on RTPS model, a generalized model, which is referred here as DCM, is trained for contact-based fingerprint deformation correction. In order to train from the contact-based fingerprint sample  $P$ , the original landmarks  $(x_{i_P}, y_{i_P})$  from the specific minutiae and the corresponding points for minimizing the localization errors  $(x_{j_P}, y_{j_P})$  are marked manually. The transformed locations  $(x'_{i_P}, y'_{i_P})$  and  $(x'_{j_P}, y'_{j_P})$  for the corresponding minutiae in ground truth sample i.e. contactless fingerprint, are also marked. The RTPS interpolate function  $f(x, y)$  can be firstly computed using these landmarks, i.e.

$$(x'_{i_P}, y'_{i_P}) = f(x_{i_P}, y_{i_P}) \quad (14)$$

All the other points of the contact-based fingerprints can be transformed using this function. Based on  $f(x_{j_P}, y_{j_P})$  and  $(x'_{j_P}, y'_{j_P})$ , the robust TPS transformation function is computed. The image sample in Fig 4 illustrates skeleton image corresponding to ridges of a *transformed* contact-based fingerprint using RTPS. Each of the fingerprints can be represented using a cylindrical model and are expected to have similar shape. Therefore corresponding contact-based fingerprint images are divided into  $n$  blocks from the fingerprint center  $(x_{c_P}, y_{c_P})$ , we assume that the deformation of the fingerprint in the same block is similar. Let  $(x_{bi}, y_{bi})$  represents the each pixel in the same block, the deformation of each pixel can be represented by the following equations,

$$\begin{aligned} (x_{bi_d}, y_{bi_d}) &= (x_{bi}, y_{bi}) - f(x_{bi}, y_{bi}) \\ &= (x_{bi}, y_{bi}) - (x'_{bi}, y'_{bi}) \end{aligned} \quad (15)$$

$$|(x_{bi_d}, y_{bi_d}) - (x_{bj_d}, y_{bj_d})| = \langle (d_x, d_y) \quad (16)$$

where  $(x_{bi_d}, y_{bi_d})$  and  $(x_{bj_d}, y_{bj_d})$  represents the deformation correction of each two pixels in the same block.  $(d_x, d_y)$  is the difference of deformation correction between each two pixels in the same block. The width  $k_P$  of the fingerprint  $P$  can be estimated from the maximum distance between, across the fingerprint image, after edge detection operation. The deformation correction of each block can be modeled as  $(\mathbf{x}_{b_d}, \mathbf{y}_{b_d})$ . For each test or unknown contact-based fingerprint sample  $Q$ , the fingerprint image center  $(x_{c_Q}, y_{c_Q})$  is computed. Let  $k_Q$  be the width of fingerprint  $Q$ . The widthwise scale of train/gallery fingerprint and query fingerprint can be estimated as,

$$sk = k_P/k_Q \quad (17)$$

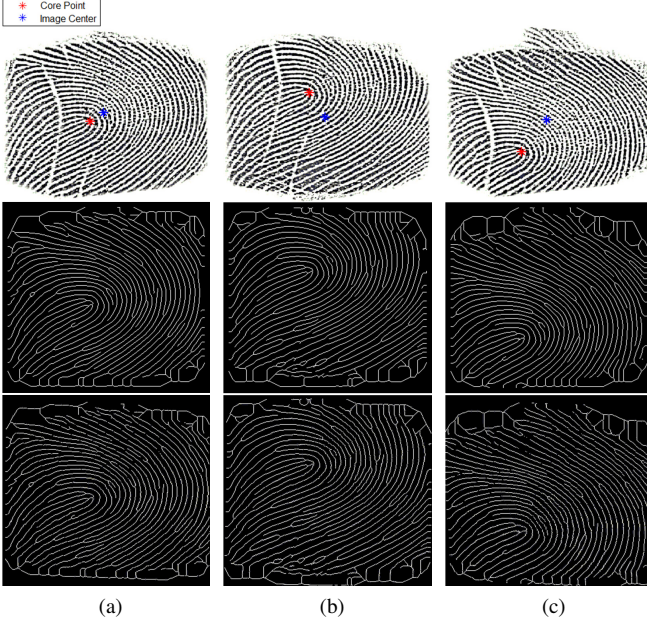


Fig. 6: Red/blue point represents core point and image center (a) Sample where center part touches the contact-based sensor with or without deformation (b) Sample where left part touches the sensor with or without deformation (c) Sample where right part touches the sensor with or without deformation.

With the consideration of widthwise scale, each query or test fingerprint can also be divided into  $n$  blocks from the fingerprint image center. The deformations in the two blocks of  $P$  and  $Q$  are considered as the same if the following conditions are met,

$$d_p = sk * d_Q \quad (18)$$

$$d_p = \sqrt{(x_{bc\_P} - x_{c\_P})^2 + (y_{bc\_P} - y_{c\_P})^2} \quad (19)$$

$$d_Q = \sqrt{(x_{bc\_Q} - x_{c\_Q})^2 + (y_{bc\_Q} - y_{c\_Q})^2} \quad (20)$$

where  $d_P$  represents the distance between each block center  $(x_{bc\_P}, y_{bc\_P})$  and fingerprint image center  $(x_{c\_P}, y_{c\_P})$  of training fingerprint  $P$ .  $d_Q$  represents the corresponding distance of  $Q$ . The transformed locations of this block can be calculated by the following equation,

$$\begin{aligned} & (x'_{bi\_Q}, y'_{bi\_Q}) \\ &= g(x_{bi\_Q}, y_{bi\_Q}) \\ &= (x_{bi\_Q}, y_{bi\_Q}) + (x_{bi\_d}, y_{bi\_d}) \\ &= (x_{bi\_Q}, y_{bi\_Q}) + (x_{bi\_P}, y_{bi\_P}) - (x'_{bi\_P}, y'_{bi\_P}) \end{aligned} \quad (21)$$

$g(x, y)$  is deformation correction function. Then for each block of  $Q$ , transformed locations of each pixels can be calculated. The marked points  $(x_{j\_P}, y_{j\_P})$  can be transformed using  $g(x, y)$  and compared with  $(x'_{j\_P}, y'_{j\_P})$  to calculate transformed points localization errors,

$$E'_{error} = \sum_{j=1}^m \|(x'_{j\_P}, y'_{j\_P}) - g(x_{j\_P}, y_{j\_P})\| \quad (22)$$

In order to ensure robustness, two contactless fingerprints and three contact-based fingerprints are used to train the

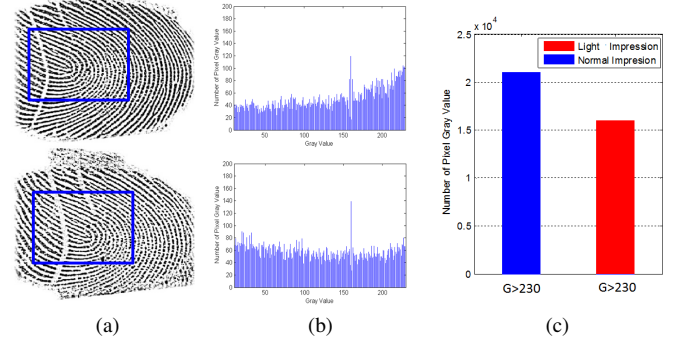


Fig. 7: (a) Typical fingerprint impression and light fingerprint impression. Automatically selected blue region ROI to exclude residual latents. (b) Histogram of fingerprint gray level (where  $G < 230$ ). (c) Respective gray level (where  $G > 230$ ) counts for two fingerprint impressions.

deformation correction models. Equations (12) and (13) are calculated in iterations to generate one optimal deformation correction model which minimizes each model's  $E'_{error}$ . A typical fingerprints alignment between the contactless skeleton fingerprints and *transformed* contact-based skeleton fingerprints with/without using proposed deformation correction models are illustrated in Fig 5.

### C. Fingerprint Impression Types and Intensity Estimation

The different spatial positions, on the different user's finger, actually touching the contact-based sensor will generate different fingerprint impression type and result in different non-linear deformations. In addition, fingerprint impression intensity can also represent the extent of fingerprint deformation. For each test or query contact-based fingerprint image, its impression type and intensity are firstly estimated. Different deformation correction model, based on the estimated impression types and intensity, are employed for the correction. We classify each of the unknown query fingerprint images into one of the three possible impression types which are automatically estimated by comparing the core point  $(x_{cp}, y_{cp})$  and image center  $(x_{ic}, y_{ic})$  of the contact-based fingerprint. The core point, i.e. reference point can be computed by the method described in [34]. We define the image center as the center of the region of interest (ROI) of the fingerprint. The ROI of a fingerprint image is also extracted automatically by implementing edge detection and the image segmentation based approach [10]. Fingerprint impression types can be determined by comparing the vertical coordinate of core point and image center.

$$-a < (y_{cp} - y_{ic}) < a \quad (23)$$

$$a < (y_{cp} - y_{ic}) < b \quad (24)$$

$$-b < (y_{cp} - y_{ic}) < -a \quad (25)$$

$$(y_{cp} - y_{ic}) > b \text{ or } (y_{cp} - y_{ic}) < -b \quad (26)$$

Equations (23)–(25) can be used to respectively ascertain whether the center part, left part or the right part of the finger touches the fingerprint sensor prominently. Parameter  $a$  and  $b$  are empirically selected as 15 and 45 for all the experiments in

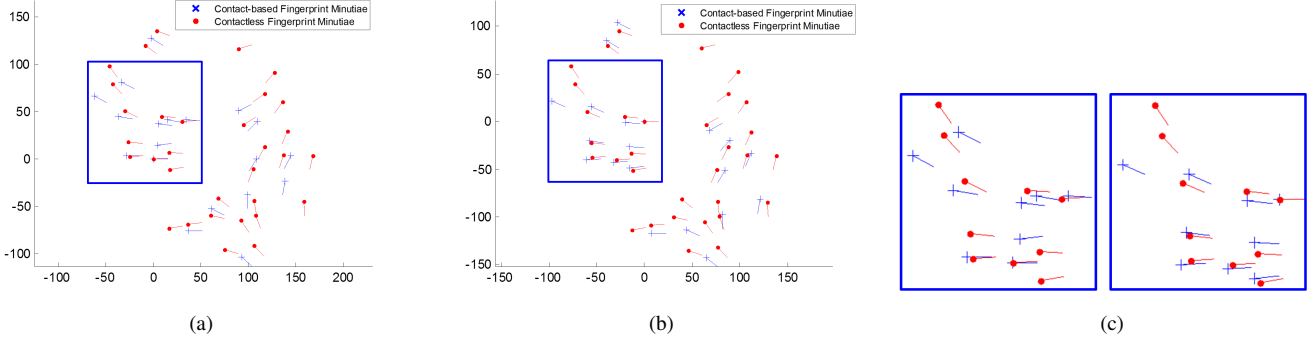


Fig. 8: Red points represent the minutiae from contactless fingerprint sample and blue crosses represent the minutiae from contact-based fingerprint sample (a) Cross minutiae matching with deformation (b) Cross minutiae matching without deformation using proposed deformation correction model (c) The details of aligned minutiae comparison in (a) and (b).

this paper. If the vertical distance between the core point and image center is very large (26), we define such types as the unknown to reduce the impact of false core point detection. Fig 6 shows the typical skeleton of fingerprint ridges for different fingerprint impression types and corresponding transformed skeleton fingerprint with/without deformation.

Fingerprint impression intensity can be estimated by calculating the average gray level  $G$  of the fingerprint. In order to exclude the influence of fingerprint latent/residue impressions on the contact-based sensor on the gray level estimation, the center region of the ROI is extracted to compute  $G$ . After testing on 40 impressions, the impressions can be divided into two types. If  $G < 100$ , we define it as normal impression. If  $G > 100$ , we define it as light impression. The sample fingerprints with normal and light impressions are illustrated in Fig 7.

#### D. Cross Matching using Deformation Correction Model

The cross matching process to match contact-based and the contactless fingerprints can be divided into offline training and the testing or the matching stage. During the training stage, based on the combination of three fingerprint impressions types and two fingerprint impressions intensity, six deformation correction models are trained. In order to alleviate the influence from undesirable imaging factors or the noise, for each model, three contact-based fingerprints and two contactless fingerprints are used to train the parameters. The average values of the parameters are selected as the final parameters. The deformation correction  $(x_d, y_d)$  of each block and the width  $k$  of each model are recorded. Minutiae from contact-based and contactless fingerprint are extracted separately using the approach described in section II.

During the matching stage, based on the fingerprint impression type and intensity estimation of each contact-based fingerprint, different deformation models are automatically selected. Let  $m_Q = [x_Q, y_Q, \theta_Q, q_Q, t_Q]$  be each minutia extracted from the contactless fingerprint image  $Q$ . Let  $m_P = [x_P, y_P, \theta_P, q_P, t_P]$  be each minutia extracted from contact-based fingerprint image  $P$ . After fingerprint impression types and intensity estimation, the widthwise scale of  $P$  and training model's fingerprint is calculated by (17). The blocks of  $P$  are

determined using (18)~(20). Each minutia can be transformed by the following equation,

$$(x'_P, y'_P) = (x_P, y_P) + (x_d, y_d) \quad (27)$$

where  $(x_d, y_d)$  represents the deformation correction of the block associated with this minutia. Then transformed minutia  $m'_P$  from  $P$  and original minutia  $m_Q$  from  $Q$  are used for fingerprints minutiae matching. The matching process is similar to the approach described in [17], [32]. The minutiae from  $P$  and  $Q$  are converted into spherical coordinate and global alignment is applied to align every minutia. The predetermined thresholds are used to determine whether each two minutiae should be considered as the matched pair or not. Then the final matching score is computed as follows:

$$S = \frac{n^2}{N_P * N_Q} \quad (28)$$

where  $n$  is the total number of cross matched minutiae pairs and  $N_P, N_Q$  are the number of minutiae in contact-based fingerprint  $P$  and contactless fingerprint  $Q$  respectively. Fig 8 illustrates the alignment and matched minutiae pairs during a typical cross matching with or without the proposed deformation correction model. It can be observed from this figure that the transformed minutiae of contact-based fingerprint can now be better aligned with the contactless fingerprint minutiae.

#### IV. MINUTIAE AND RIDGES MATCHING

For fingerprint sensor interoperability problem, the spurious or missing minutiae can seriously degrade the cross matching performance. This aspect is particularly problematic when these minutiae are extracted from the contact-based and contactless fingerprint sensors and the reason can be attributed respectively to the imaging resolution/capability of different sensors and higher susceptibility to noise resulting from high degree of freedom in the contact-based fingerprint sensors. Therefore in addition to the minutiae feature, we also investigated the use of minutiae related ridges and attempted to improve accuracy for the cross matching. Unlike the work in [17], [32] where the minutiae and related ridges are employed for the alignment or matching, we only use minutiae for the alignment and related ridges are considered as an additional feature during the final stage of cross matching.

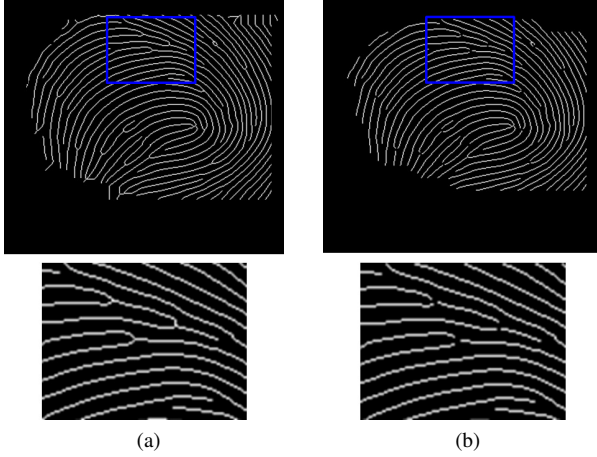


Fig. 9: Sample fingerprint image after thinning in (a) and respective image after processing in (b) for ridge matching.

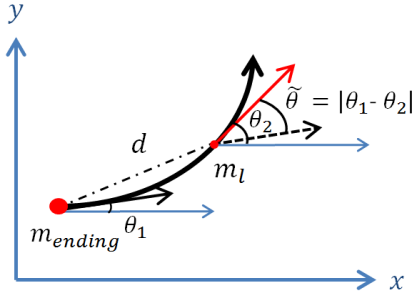


Fig. 10: Matching fingerprint ridge features where  $m_l$  represents any point on the ridge.  $d$  represents the distance between minutiae ending to this point.  $\tilde{\theta}$  is minutiae orientation difference.

#### A. Minutia and Related Ridges Extraction for Matching

In order to extract minutiae related ridges, the traditional minutiae extraction algorithm is implemented. The Gabor filter is used to enhance the image which is followed by the binarization and thinning to generate the ridge image. The preprocessing approach for the ridge image is similar to as in [35]. The closed ridges (small holes) are disconnected and short ridges are removed after preprocessing. The bifurcation minutiae related ridges are split into three ridges. Fig 9 illustrates typical preprocessing of the fingerprint ridges.

Let  $(m_e, m_b)$  be the original minutiae ending and bifurcation and  $m'_b$  be the split bifurcation point. For each minutia, the related ridges  $(r_e, r'_b)$  are recorded. The duplicated ridges, i.e. one ridge that contains both minutia ending and split minutia bifurcation, will only be considered as one ridge. Based on the extracted minutia and the related ridges, ridge features can be localized as  $(\mathbf{L}, \mathbf{D}, \tilde{\Theta})$ , where  $L = (x_r, y_r)$  is the position of each point of the ridge,  $\mathbf{D}$  represents the distance from each point on the ridge  $\mathbf{L}$  to the position of minutia  $m_e$  or  $m'_b$  while  $\tilde{\Theta}$  is orientation differences between each point on the ridge and the minutia. Let  $m_Q$  represent a sample minutia extracted from the contactless fingerprint image  $Q$ . Let  $m_P$  represent a sample minutia extracted from the contact-based fingerprint image  $P$ . Fingerprint minutiae alignment and matching method is applied to find

matched minutiae pairs, say,  $\mathbf{m}_Q = (m_{q1}, \dots, m_{qk}, \dots, m_{qn})$  and  $\mathbf{m}_P = (m_{p1}, \dots, m_{pk}, \dots, m_{pn})$  where  $n$  is the number of matched minutiae pairs. For each matched minutiae pair, the features of related ridges are used for computing the ridge matching score. For example, the related ridge  $r_{pk}$  of matched minutia  $m_{qk}$  from  $Q$  is  $(\mathbf{L}_{qk}, \mathbf{D}_{qk}, \tilde{\Theta}_{qk})$  and the related ridge  $r_{qk}$  of matched minutia  $m_{pk}$  from  $P$  is  $(\mathbf{L}_{pk}, \mathbf{D}_{pk}, \tilde{\Theta}_{pk})$ . If the difference between  $r_{pk}$  and  $r_{qk}$  is smaller than a given threshold, i.e.,

$$\begin{aligned} \Delta \mathbf{L} &= |\mathbf{L}_{pk} - \mathbf{L}_{qk}| \\ \Delta \mathbf{D} &= |\mathbf{D}_{pk} - \mathbf{D}_{qk}| \\ \Delta \tilde{\Theta} &= |\tilde{\Theta}_{pk} - \tilde{\Theta}_{qk}| \end{aligned} \quad (29)$$

If  $\Delta \mathbf{L} < th_{\mathbf{L}}$ ,  $\Delta \mathbf{D} < th_{\mathbf{D}}$  and  $\Delta \tilde{\Theta} < th_{\tilde{\Theta}}$ , two related ridges can be considered as matched. The minutiae type is also considered into account when the related ridges are used for the matching. For minutiae bifurcation related three ridges, if two of them can be matched, we consider such bifurcation related ridges as being matched. However for the minutiae ending and bifurcation related ridges, if one of bifurcation related ridges can be matched with minutiae ending related ridges, this ridge pair is considered as being matched. The match score from the ridges are computed as follows:

$$S = \frac{n_r}{n} \quad (30)$$

$$S_r = \omega_{11} * S_{e_{-r}} + \omega_{12} * S_{b_{-r}} + \omega_{13} * S_{be_{-r}} \quad (31)$$

$$\omega_{11} + \omega_{12} + \omega_{13} = 1 \quad (32)$$

where  $n_r$  is number of matched ridges.  $\omega_{11}$ ,  $\omega_{12}$  and  $\omega_{13}$  are the weight for the types of matched ridges.  $S_{e_{-r}}$  is the matching score of minutia ending related ridges.  $S_{b_{-r}}$  is the matching score of minutia bifurcation related ridges.  $S_{be_{-r}}$  is the match score of minutia bifurcation and ending related ridges. The final or consolidated match score between the fingerprints is computed as follows:

$$S_{final} = \omega_1 * S_{minutiae} + \omega_2 * S_r \quad (33)$$

where  $S_{minutiae}$  is matching score using minutia while  $\omega_1$  and  $\omega_2$  represent the weight for the minutiae and related ridges. Fig 10 illustrates the sample minutia related ridge and its features for the matching.

#### B. Ridge Matching using Deformation Correction Model

In addition to investigating the deformation correction for fingerprint minutiae, the deformations in minutiae related ridges can also be corrected by using the proposed model. For each of the contact-based fingerprint image  $P$ , based on the respective fingerprint impression type and intensity estimation, different deformation correction models are automatically selected. Besides minutiae correction for  $m_p$ , each point on the minutia related ridge  $r_p$  can also be transformed by the proposed model. The transformed minutiae  $m'_p$  and transformed related ridges  $r'_p$  are then used for the matching. The deformation correction and ridge matching strategy has been detailed earlier in section III-D and section IV-A.

TABLE I: The equal error rate from different matching approaches

Database	Experiments	Equal Error Rate
<b>PolyU Contactless to Contact-based Fingerprint Database [20]</b>	Contact-based fingerprint matching using [38]	10.56%
	Contact-based fingerprint matching using [15]	7.42%
	Contact-based fingerprint matching using [39]	11.90%
	Contact-based fingerprint matching using <b>TPS+DCM</b>	<b>5.72%</b>
	Contact-based fingerprint matching using <b>RTPS+DCM</b>	<b>4.46%</b>
	Cross matching using [38]	36.30%
	Cross matching using [15]	25.37%
	Cross matching using [39]	38.90%
	Cross matching using minutiae with <b>TPS+DCM</b>	<b>18.12%</b>
	Cross matching using minutiae & ridge with <b>TPS+DCM</b>	<b>16.14%</b>
	Cross matching using minutiae with <b>RTPS+DCM</b>	<b>15.35%</b>
Cross matching using minutiae & ridge with <b>RTPS+DCM</b>	<b>14.33%</b>	
<b>Benchmark 2D/3D Fingerprint Database [37]</b>	Cross matching using [38]	40.34%
	Cross matching using [15]	26.83%
	Cross matching using [39]	31.28%
	Cross matching using minutiae with <b>RTPS+DCM</b>	<b>19.81%</b>

## V. EXPERIMENTAL RESULTS

In this section we detail experimental results to ascertain the usefulness of matching contactless to contact-based fingerprints using the approach described in previous section. In this work, a dataset consisting of 1800 2D contactless fingerprint images and corresponding 1800 2D contact-based fingerprints from 300 distinct client fingers was acquired from the volunteers in or visiting our university. Six fingerprint image samples were acquired from each of the client fingers. The contactless 2D fingerprint images are acquired using a low-cost camera and lens. Corresponding 2D contact-based fingerprints were acquired using URU 4000 fingerprint reader [36] which meets FBI/NIST [38] specifications. Like many other references on contactless fingerprint matching, e.g. [25], [26], [27], [37]. It is assumed that user is cooperative, has an interest in positive authentication, and therefore the imaging distortion due to the rotation or incorrect placement of fingerprint can be assumed smaller. All the images in this database are employed for the test experiments. Several other contactless and contact-based fingerprints using the same set of sensor were acquired (also available in [20]) and used for training the deformation correction model. In addition to the performance evaluation using this database, the experimental results are also reported by using another publicly available database provided recently made available by the authors from reference [37]. This dataset contains 1500 fingers, for each finger there are two contactless fingerprint samples and four corresponding contact-based fingerprint samples. In our experiments the 1000 fingers of the dataset were used for the performance evaluation. All these images from 1000 fingers in this database are employed for the test experiments. Several other contactless and contact-based fingerprint images from the rest 500 fingers are used for training the deformation correction model. The programs of our experiments were run on a PC with i7-4770 CPU under Windows 7. The original resolution of acquired 2D contactless fingerprint images and contact-based fingerprint was respectively 1400×900 and 356×328 with 500 dpi respectively. The original resolution of contactless fingerprint images in [37] is 1024×1280 and

corresponding contact-based fingerprint resolution is 640×480 with 500 dpi respectively.

We also comparatively evaluated the performance from the algorithm described in section III and IV and using other popular or competing fingerprint matching algorithms detailed in the literature. We firstly evaluated the fingerprint matching performance from only using the contact-based fingerprints images. The deformation in each of the contact-based fingerprint images is corrected by comparing with the respective contactless fingerprints using different methods. The generalized deformation correction model is trained using independent contact-based fingerprints and corresponding contactless fingerprint images that are not *available* in the test database. This verification experiment generated 4500 (300×15) genuine and 1614600 (300×6×299×3) imposter matching scores. The proposed algorithm is compared with the method proposed in [15], conventional fingerprint matching algorithm provided by NIST [38] and Minutia Cylinder-Code (MCC) method proposed in [39]. In order to make fair comparison with the method in [15] and achieve the best possible performance for the benchmarking, we first correct the contact-based fingerprint deformations based on the *respective contactless fingerprint* from the same subject using minutiae-based approach in [15]. Then contact-based fingerprint (with deformation correction) matching experiment is performed. The average number of minutiae generated using proposed method from contactless fingerprint is 28.83 and from contact-based fingerprint is 29.79. The average number of minutiae generated using NBIS matcher implemented by NIST [38] from contactless fingerprint is 33.57 and from contact-based fingerprint is 41.36. These comparative experimental results are presented in Fig 11 (a) using the ROC. These results suggest that the contact-based fingerprint matching using the proposed deformation correction model and the robust thin-plate spline ( $ERR = 4.46\%$ ) can achieve more accurate performance than those from using deformation correction model and thin-plate spline ( $ERR = 5.72\%$ ), method in [38] ( $ERR = 7.42\%$ ), method in [15] ( $ERR = 10.56\%$ ) and method in [39] ( $ERR = 11.90\%$ ).

The second sets of experiment are performed to evaluate

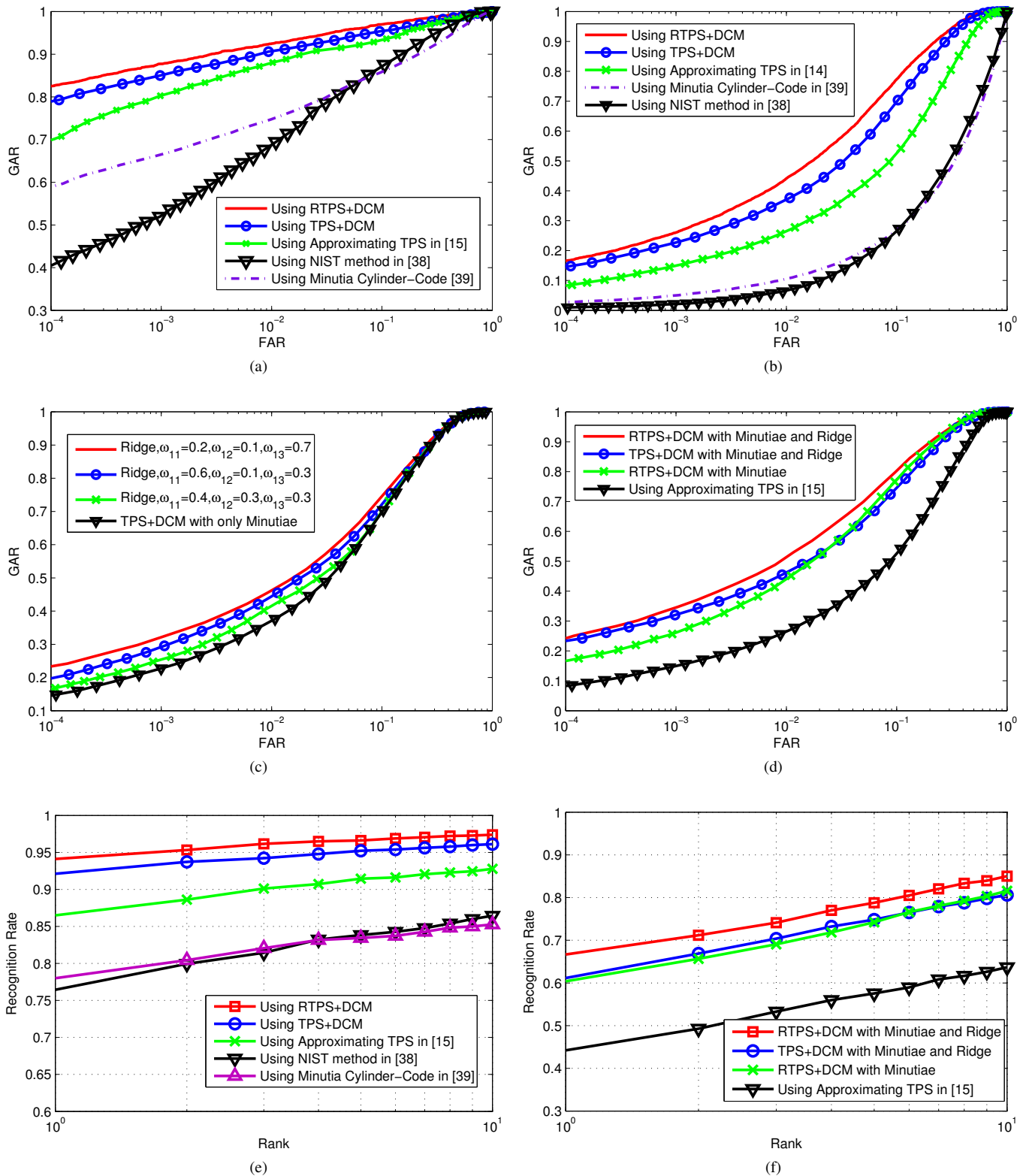


Fig. 11: Comparative experimental results using PolyU Contactless to Contact-based Fingerprint Database [20] (a) ROC curve for matching contact-based fingerprints using proposed method, the method in [15], the method in [38] and the method in [39] (b) ROC curve for cross matching using deformation correction model, the method in [15], the method in [38] and the method in [39] (c) ROC curve for cross matching using deformation correction model and ridge features with different parameter (d) ROC curve for cross matching using proposed method with minutiae and ridge features, and the other methods (e) CMC curve for matching contact-based fingerprints using proposed method, the method in [15], the method in [38] and the method in [39] (f) Comparison CMC curve for cross matching using proposed algorithm and other methods

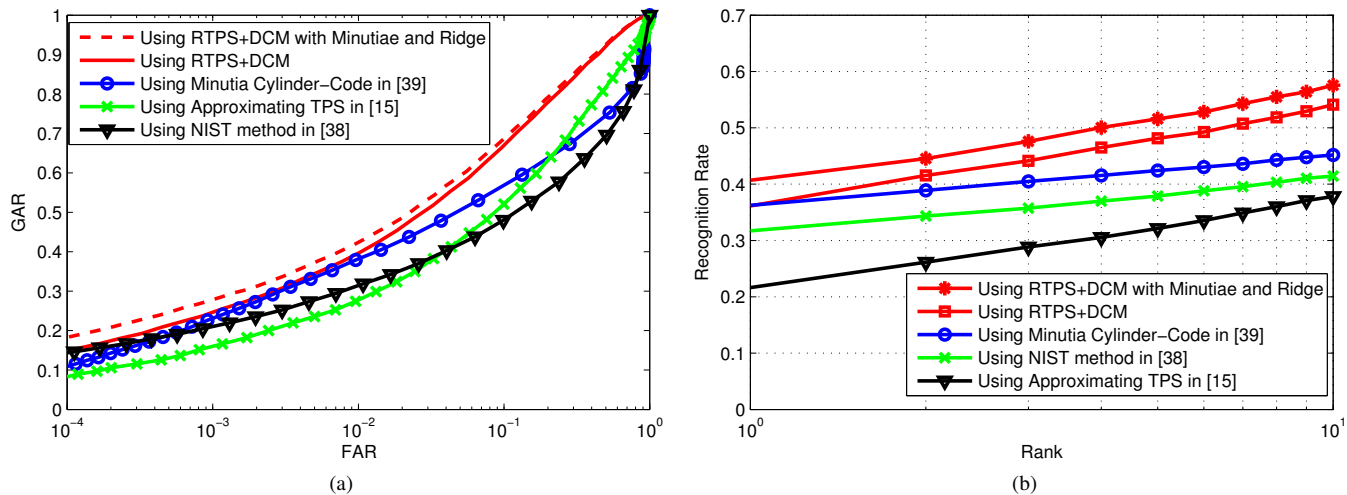


Fig. 12: Comparative experimental results using benchmark 2D/3D fingerprint database [37] (a) ROC curve for cross matching using proposed method, the method in [15], the method in [38] and the method in [39] (b) CMC curve for cross matching using proposed method, the method in [15], the method in [38] and the method in [39]

TABLE II: The rank-one recognition accuracy from different matching approaches

Database	Experiments	Rank-1 accuracy
PolyU Contactless to Contact-based Fingerprint Database [20]	Contact-based fingerprint matching using [38]	76.44%
	Contact-based fingerprint matching using [15]	86.50%
	Contact-based fingerprint matching using [39]	78.02%
	Contact-based fingerprint matching using <b>TPS+DCM</b>	<b>92.11%</b>
	Contact-based fingerprint matching using <b>RTPS+DCM</b>	<b>94.11%</b>
	Cross matching using [38]	16.61%
	Cross matching using [15]	44.22%
	Cross matching using [39]	19.50%
	Cross matching using minutiae with <b>TPS+DCM</b>	<b>54.55%</b>
	Cross matching using minutiae & ridge with <b>TPS+DCM</b>	<b>61.17%</b>
	Cross matching using minutiae with <b>RTPS+DCM</b>	<b>60.39%</b>
	Cross matching using minutiae & ridge with <b>RTPS+DCM</b>	<b>66.67%</b>
Benchmark 2D/3D fingerprint database [37]	Cross matching using [38]	27.30%
	Cross matching using [15]	21.56%
	Cross matching using [39]	36.15%
	Cross matching using minutiae with <b>RTPS+DCM</b>	<b>36.25%</b>

the proposed algorithm on cross matching using contactless and contact-based fingerprints. The scales have been normalized between the images from contact-based and contactless fingerprint for matching using method [15], NBIS and MCC matcher. This set of experiments generated 10800 (300×36) genuine matching scores and 3229200 (300×6×299×6) imposter matching scores. The sample images for the alignment in Fig 8 suggest that contact-based fingerprint can be better aligned with the contactless fingerprint by using proposed deformation correction model. As a result, the average matching score for this (Fig 8) cross-matching sample has been improved from 0.3194 to 0.6079. As can be observed from the ROC curve in Fig 11 (b), the proposed method offers superior matching results than the method in [15], [38] and [39]. The EER from the cross matching experiment using proposed DCM and RTPS is 15.35%, using proposed DCM and TPS is 18.12% and it is 25.37% using the method in [15].

We also performed experiments to ascertain further improvement in the performance for cross-matching of contactless and contact-based fingerprints using the minutiae and

related ridges approach as discussed in section IV-B. These experimental results are shown in Fig 11 (c) using ROC, along with related parameters employed for such score level combination. The EER is decreased from 18.12% to 16.31% combining the ridge features with the minutiae features. The result in Fig 11 (d) illustrates comparative ROC for the cross-matching using proposed method that combines with ridge feature and other methods. In combination with the ridge features, the proposed RTPS and DCM method achieves best performance with 14.33% *EER*.

We also performed experiments to ascertain the recognition performance and the CMC (cumulative match characteristics) curve and the average rank-one accuracy were used to evaluate the performance for the recognition problem. The CMC curve Fig 11 (e) illustrates the matching performance by only using contact-based fingerprints. The comparative cross-matching results using the proposed algorithm and using other methods are shown in Fig 11 (f). These experimental results also suggest superior performance using the proposed method.

At last we also present the experimental results using

the dataset in [37] and ascertain the performance from the proposed algorithm. The average number of minutiae generated using the proposed method from contactless fingerprint is 31.97. The average number of minutiae generated using NBIS matcher implemented by NIST [38] from contactless fingerprint is 38.57 and from contact-based fingerprint is 42.91. The comparative ROC and CMC for the cross matching performance using the proposed methods and other competing methods is illustrated in Fig 12 (a) and (b). This verification experiment generated 8000 ( $1000 \times 2 \times 4$ ) genuine matching scores and 7992000 ( $1000 \times 4 \times 999 \times 2$ ) imposter matching scores. The EER for the cross-matching using proposed DCM and RTPS is 19.81%, using the method in [15] is 26.83% , using the method in [38] is 40.34% and using the method in [39] is 31.28%. The rank-one accuracy is 36.25% for the cross-matching using proposed DCM and RTPS, using the method in [38] is 27.30% , using the method in [15] is 21.65% and using method in [39] is 36.15% . Table 1 and Table 2 consistently suggest the improvement in EER and (rank-one) recognition accuracy using proposed method on both the datasets. The identification experimental results, using the proposed method, on this public dataset also indicate superior performance.

## VI. CONCLUSIONS AND FURTHER WORK

This paper has described the development of deformation correction model for efficiently and accurately matching contactless and contact-based conventional fingerprint images. We proposed a robust thin-plate spline model that was incorporated for the correction of deformations to address contact-based and contactless sensor interoperability problems. The proposed model (section III) is generalized, does not rely on the quality of extracted minutiae and has shown to achieve significant improvement in the alignment of contact-based and contactless fingerprints. A method to estimate contact-based fingerprint impression type and intensity is also introduced. The experimental results are reported using a dataset that had contact-based fingerprints and the corresponding contactless fingerprints. The experimental results using this publicly available database illustrate that the proposed method can achieve superior matching performance than the other competing methods [15], [38] and [39]. Our efforts to incorporate minutiae and the simultaneously made available respective ridge features also yielded promising results. Such experimental results were presented in section five and illustrate further improvement in performance by incorporating the minutiae and ridge based features for the cross fingerprint matching.

The deformation correction model developed in Section III of this paper incorporates a model that requires training samples from contact-based and contactless fingerprint sensors. In order to ensure interoperability of algorithm, such requirement can be relaxed when fingerprint sensors comply with some standard. However, the contactless fingerprint sensors used from two public databases in this work are very different, do not meet any common standard and therefore do not meet expectation for cross-database performance evaluation. Sensor interoperability using contact-based and contactless fingerprint is a challenging problem but needs to be addressed to advance

acceptability of emerging contactless fingerprint technologies. Despite significant improvement in the accuracy for such matching, the current cross-matching error rates are not yet attractive for the deployment. Our experimental results also illustrate significant improvement over the methods in the literature. However the achieved error rates need to be further improved.

The databases employed in this work makes reasonable assumption that the user is cooperative during contactless fingerprint imaging and such cooperation is often expected from contactless biometrics systems like during the iris imaging. Perspective distortion in contactless images, specifically when user is less-cooperative, can further degrade the matching performance. Therefore, automated detection and correction of perspective distortion in contactless fingerprint images is expected to reduce the error rates. In addition, usage of more robust core detection algorithm and incorporating more powerful matching strategy can also reduce error rates and are suggested for the further work. Deep learning based approaches have the potential to achieve more accurate fingerprint recognition [43] and such methods can also be explored for contactless to contact-based fingerprint matching in the further work.

## REFERENCES

- [1] A. K. Jain and A. Kumar, "Biometric recognition: an overview," in *Second Generation Biometrics: The Ethical, Legal and Social Context*. Springer, 2012, pp. 49–79.
- [2] D. Maltoni, D. Maio, A. Jain, and S. Prabhakar, *Handbook of fingerprint recognition*. Springer Science & Business Media, 2009.
- [3] A. Ross and A. Jain, "Biometric sensor interoperability: A case study in fingerprints," in *Biometric authentication*. Springer, 2004, pp. 134–145.
- [4] Aadhaar project, [http://www.stqc.gov.in/sites/upload\\_files/stqc/files/Authlist\\_27042015\\_v2.1.2\\_alphabeticalorder%20.pdf](http://www.stqc.gov.in/sites/upload_files/stqc/files/Authlist_27042015_v2.1.2_alphabeticalorder%20.pdf), accessed 2016.
- [5] Ten-print fingerprint scanner, <http://www.bioenabletech.com/ten-print-fingerprint-scanner/>, accessed 2016.
- [6] P. Krishnasamy, S. Belongie, and D. Kriegman, "Wet fingerprint recognition: Challenges and opportunities," in *Proc. IJCB*, 2011, pp. 1–7.
- [7] MorphoWave Tower, <http://www.morpho.com/>, accessed 2016.
- [8] A. Kumar and Y. Zhou, "Contactless fingerprint identification using level zero features," in *Proc. CVPRW*, 2011, pp. 114–119.
- [9] G. Parziale and Y. Chen, "Advanced technologies for touchless fingerprint recognition," in *Handbook of Remote Biometrics*. Springer, 2009, pp. 83–109.
- [10] A. Kumar and C. Kwong, "Towards contactless, low-cost and accurate 3d fingerprint identification," in *Proc. CVPR*, 2013, pp. 3438–3443.
- [11] C. Lin and A. Kumar, "On cross sensor interoperability for fingerprint identification," *No. COMP-K-22*, Tech. Rep., May 2016.
- [12] Z. M. Kovács-Vajna, "A fingerprint verification system based on triangular matching and dynamic time warping," *IEEE Trans. Pattern Anal. Mach. Intell.*, pp. 1266–1276, 2000.
- [13] R. Cappelli, D. Maio, and D. Maltoni, "Modelling plastic distortion in fingerprint images," in *Proc. ICAPR 2001*. Springer, 2001, pp. 371–378.
- [14] A. Ross and R. Nadgir, "A thin-plate spline calibration model for fingerprint sensor interoperability," *IEEE Trans. Knowledge and Data Engineering*, pp. 1097–1110, 2008.
- [15] A. M. Bazen and S. H. Gerez, "Fingerprint matching by thin-plate spline modelling of elastic deformations," *Pattern Recognition*, pp. 1859–1867, 2003.
- [16] A. Ross, S. Dass, and A. Jain, "A deformable model for fingerprint matching," *Pattern Recognition*, pp. 95–103, 2005.
- [17] A. Ross, S. C. Dass, and A. K. Jain, "Fingerprint warping using ridge curve correspondences," *IEEE Trans. Pattern Anal. Mach. Intell.*, pp. 19–30, 2006.
- [18] F. L. Bookstein, "Principal warps: Thin-plate splines and the decomposition of deformations," *IEEE Trans. Pattern Anal. Mach. Intell.*, pp. 567–585, 1989.

- [19] K. Rohr, M. Fornefett, and H. S. Stiehl, "Approximating thin-plate splines for elastic registration: Integration of landmark errors and orientation attributes," in *Information Processing in Medical Imaging*. Springer, 1999, pp. 252–265.
- [20] Weblink for downloading *PolyU Contactless to Contact-based Fingerprint Database*, <http://www.comp.polyu.edu.hk/~csajaykr/fingerprint.html/>.
- [21] S. S. Wood and C. L. Wilson, *Studies of plain-to-rolled fingerprint matching using the NIST algorithmic test bed (ATB)*. US Department of Commerce, Technology Administration, National Institute of Standards and Technology, 2004.
- [22] F. Alonso-Fernandez, R. N. Veldhuis, A. M. Bazen, J. Fierrez-Aguilar, and J. Ortega-Garcia, "Sensor interoperability and fusion in fingerprint verification: A case study using minutiae-and ridge-based matchers," in *Proc. ICARCV'06*, 2006, pp. 1–6.
- [23] S. K. Modi, "Analysis of fingerprint sensor interoperability on system performance," Purdue University West Lafayette, Tech. Rep., 2008.
- [24] Y. Chen, G. Parziale, E. Diaz-Santana, and A. K. Jain, "3d touchless fingerprints: compatibility with legacy rolled images," in *Biometric Consortium Conference, 2006 Biometrics Symposium: Special Session on Research at the*, 2006, pp. 1–6.
- [25] Y. Chen, "Extended feature set and touchless imaging for fingerprint matching," Ph.D. dissertation, Doctoral dissertation, Michigan State University, 2009.
- [26] Azimuth Inc., "Evaluation of contact versus contactless fingerprint data (final report v2)," Report No.245146, I. ManTech Advanced Systems International, DOJ Office of Justice Programs, 2014.
- [27] L. Ericson and S. Shine, "Evaluation of contactless versus contact fingerprint data, phase 2 (version 1.1)," Report No. 249552, I. ManTech Advanced Systems International, DOJ Office of Justice Programs, 2015.
- [28] A. W. Senior and R. M. Bolle, "Improved fingerprint matching by distortion removal," *IEICE Trans. on Inf. and Systems*, pp. 825–832, 2001.
- [29] S. M. Pizer, E. P. Amburn, J. D. Austin, R. Cromartie, A. Geselowitz, T. Greer, B. ter Haar Romeny, J. B. Zimmerman, and K. Zuiderveld, "Adaptive histogram equalization and its variations," *Computer vision, graphics, and image processing*, pp. 355–368, 1987.
- [30] L. Xue, F. L. Stahura, J. W. Godden, and J. Bajorath, "Fingerprint scaling increases the probability of identifying molecules with similar activity in virtual screening calculations," *Journal of Chemical Information and Computer Sciences*, pp. 746–753, 2001.
- [31] J. M. Guo, C. X. Ren, and Y. X. Wu, "Fingerprint scaling for sensor interoperability," in *Applied Mechanics and Materials*, vol. 303. Trans Tech Publ, 2013, pp. 908–911.
- [32] A. Jain, L. Hong, and R. Bolle, "On-line fingerprint verification," *IEEE Trans. Pattern Anal. Mach. Intell.*, pp. 302–314, 1997.
- [33] ISO/IEC, "Information technology–biometric data interchange formats–19794-part 2: Finger minutiae data," 2005.
- [34] A. K. Jain, S. Prabhakar, L. Hong, and S. Pankanti, "Filterbank-based fingerprint matching," *IEEE Trans. Image Process.*, pp. 846–859, 2000.
- [35] J. Feng, Z. Ouyang, and A. Cai, "Fingerprint matching using ridges," *Pattern Recognition*, pp. 2131–2140, 2006.
- [36] Crossmatch, <http://www.crossmatch.com/products/>, accessed 2016.
- [37] W. Zhou, J. Hu, I. Petersen, S. Wang, and M. Bennamoun, "A benchmark 3d fingerprint database," in *Proc. FSKD*. IEEE, 2014, pp. 935–940.
- [38] C. I. Watson, M. D. Garris, E. Tabassi, C. L. Wilson, R. M. McCabe, S. Janet, and K. Ko, "User's guide to nist biometric image software (nbis)," NIST, 2007.
- [39] R. Cappelli, M. Ferrara, and D. Maltoni, "Minutia cylinder-code: A new representation and matching technique for fingerprint recognition," *IEEE Trans. Pattern Anal. Mach. Intell.*, pp. 2128–2141, 2010.
- [40] C. Lin and A. Kumar, "Improving cross sensor interoperability for fingerprint identification," in *Proc. ICPR*, 2016, pp. 943–948.
- [41] W. Zhou, J. Hu, S. Wang, I. Petersen, and M. Bennamoun, "Performance evaluation of large 3d fingerprint databases," *Electronics Letters*, vol. 50, no. 15, pp. 1060–1061, 2014.
- [42] R. D. Labati, A. Genovese, V. Piuri, and F. Scotti, "Contactless fingerprint recognition: a neural approach for perspective and rotation effects reduction," in *Computational Intelligence in Biometrics and Identity Management (CIBIM), IEEE Workshop on*, 2013, pp. 22–30.
- [43] F. Zhang and J. Feng, "High-Resolution Mobile Fingerprint Matching via Deep Joint KNN-Triplet Embedding," in *AAAI*, 2017, pp. 5019–5020.